The International Journal of Advanced Manufacturing Technology (2019) 102:3165–3180
https://doi.org/10.1007/s00170-019-03432-8

ORIGINAL ARTICLE

Multi-objective and many objective design of plastic injection molding process

Alejandro Alvarado-Iniesta[1] · Oliver Cuate[2] · Oliver Schütze[3]

Received: 5 December 2018 / Accepted: 6 February 2019 / Published online: 12 February 2019

Abstract
Plastic injection molding is one of the most used manufacturing processes capable of producing flexible and economical parts at a large scale. Since this is a highly complex process, it is a natural consequence that there are many conflicting objectives that are worth considering in the design of such process. Problems where more than three objectives are being considered at the same time are termed many objective problems (MaOPs) in literature. Unlike for multi-objective problems (MOPs, problems with two or three objectives), there is no consensus of how to find ideal solutions for general MaOPs. In this paper, the multi-objective and many objective design of a plastic injection molding process is addressed. To accomplish this task, the two main contributions of this work are as follows: first, a new optimization model that contains up to seven objectives is proposed. That is, for the first time, it is considered the many objective design of a plastic injection process. Second, the usefulness of the Pareto Explorer, a global/local exploration tool for MaOPs, in the current context is demonstrated. For this, the complete seven-objective optimization problem on several selected scenarios related to the hypothetical decision making of a plastic gear is considered.

Keywords Plastic injection molding · Multi-objective optimization · Many objective optimization · Decision making

1 Introduction

Plastic injection molding (PIM) is one of the major processes in polymer processing capable of producing parts with complex shapes at a relatively low cost. Many daily use products, e.g., electronics devices, appliances, and packaging, rely on the technology and production of the PIM industry. PIM is a process that consists of six phases: clamping, filling, packing, cooling, opening, and ejecting. All phases are not independent with each other; an improper clamping setting may result in a failing filling phase, and so on, affecting the performance of the overall process. Usually, the performance of a PIM process is measured by outcomes such as qualities of the parts, i.e., appearance characteristics, and functional properties [27, 28, 32, 52, 53, 62], and productivity indicators, e.g., production cost, cycle time, and energy consumption [27, 33, 61]. Undoubtedly, there is a trade-off between quality and productivity (e.g., a high-quality product rarely results in a low production cost and vice versa); therefore, the PIM process can be viewed as a problem where several incommensurate and competing outcomes need to be simultaneously satisfied.

Such problems are termed *multi-objective optimization problems* (MOPs) in literature if two or three objectives are being considered, and *many objective optimization problems* (MaOPs) if more than three objectives are under consideration. Although MOPs and MaOPs are in principle defined equally—k objectives have to be optimized concurrently—these two distinct terms are used since the solution sets of M(a)OPs, the so-called Pareto sets, respectively, their images, the Pareto fronts, typically form

✉ Alejandro Alvarado-Iniesta
alejandro.alvarado@uacj.mx

Oliver Cuate
ocuate@computacion.cs.cinvestav.mx

Oliver Schütze
schuetze@cs.cinvestav.mx

[1] Department of Industrial and Manufacturing Engineering, Universidad Autonóma de Ciudad Juárez, Ciudad Juárez, Chihuahua, Mexico

[2] Computer Science Department, Cinvestav-IPN, Mexico City, Mexico

[3] Department of Applied Mathematics and Systems, Dr. Rodolfo Quintero Chair, UAM Cuajimalpa, Mexico City, Mexico

objects of dimension $k-1$. Hence, while it is possible to compute suitable approximations of the Pareto set for MOPs, this is not the case any more for MaOPs.

In this work, it is argued that in a PIM design, there are—depending on the scenario—up to seven objectives worth considering. This means, all of those seven objectives may lead to significant changes in the final design, and all of them are in conflict to each other. Hence, it makes sense to consider the MaOP that is defined by all of these seven objectives. As mentioned above, it is not possible any more to compute the entire solution set for such a problem. As alternative, in this work, the recently proposed Pareto Explorer (PE) framework is considered [47], a global/local approach that allows to identify a suitable solution for the given scenario that is capable of incorporating the decision makers (DM) preferences. More precisely, PE computes a sequence of candidate solutions in two steps: first, an initial solution x_0 is computed via a global method (e.g., an evolutionary reference point method [17]) that ideally already roughly meets the criteria of the DM. In a next step, a local movement along the Pareto set/front starting from x_0 is performed based on the DMs preferences. These preferences can be articulated via directions in those the search has to be performed along the solution set. The directions can either be defined in decision variable or objective space, or in the weight space. The second step hence allows to interactively explore the Pareto landscape around x_0 and hopefully helps to find the ideal solution for the DM according to the given problem. This will be demonstrated on several selected scenarios related to the many objective design of a particular plastic gear.

The remainder of the paper is organized as follows: In Section 2, the background required for the understanding of this work is stated. In Section 3, the seven-objective MaOP to be considered for PIM design is presented , and introduced the case study that it is going to be considered for the computations. In Section 4, some numerical results are presented. For this, some MOPs are investigated with two and three objectives that will be among others to show the importance of all individual objectives. Next, the Pareto Explorer is applied on four selected hypothetical scenarios to demonstrate how to numerically solve a many objective PIM design. Finally, conclusions are addressed in Section 5 and possible paths of future research are given.

2 Background

2.1 Plastic injection molding

Quality and productivity of PIM depends on the appropriate integration of factors such as product design, mold design, material selection, and process parameters setting. Once mold and material are chosen, the only factor that can be adjusted are the process parameters (a change of the mold design can be considerably costly). Process parameters setting is recognized as a crucial factor to obtain high-quality products efficiently and economically [52]. This paper focuses on process parameters optimization from a many objective optimization perspective. Although there are several process parameters and outcomes of interest involved in the PIM process, in the next sub-sections, the ones considered in this work are briefly described . A full description and further details about PIM process can be found in [9, 10, 45].

In the last years, several works have addressed the multi-objective design of PIM processes, where mainly surrogate models have been utilized to build the model. For instance, Tian et al. [52] considered a three-objective problem by using Taguchi as sample collection method and response surface methodology (RSM) as surrogate model and combined with the multi-objective evolutionary algorithm NSGA-II [16] to obtain the optimal process parameter combinations. Similarly, Park et al. [41] employed a RSM surrogate model and NSGA-II for a bi-objective injection molding problem. Liu et al. [32] addressed the manufacturing of a plastic optical lens. In this work, they have used the Taguchi method for collecting data, artificial neural networks (ANNs), and support vector machines (SVMs), and, finally, applied NSGA-II to obtain the Pareto optimal set. Kitayama et al. [26] employed a Latin hypercube design for data collection, and used a radial basis ANN to model the outcomes; finally, they have used the weighted l_p-norm method for finding Pareto optimal solutions. Villarreal-Marroquin et al. [55] combined physical and simulated data to build a calibrated predictor using Bayesian methodology to optimize a three-objective problem. Other works (e.g., [27, 33, 61, 62]) are quite similar to the ones described above. Nevertheless, none of these works have addressed the optimization of the injection molding process with more than three objectives, (i.e., $k > 3$). In addition, most of the works focus their search on finding an approximation of the Pareto front/set. In contrast, this paper considers a seven-objective problem and focuses on the related decision-making process via guiding the search along user-specified directions along the Pareto set/front of the given problem.

2.2 Multi-objective optimization

A continuous multi-objective optimization problems (MOP) can mathematically be expressed as

$$\min_{x \in Q} F(x), \tag{1}$$

where $Q \subset \mathbb{R}^n$ is the domain and $F : Q \to \mathbb{R}^k$ is defined as the vector of the objective functions

$$F(x) = (f_1(x), \ldots, f_k(x))^T, \tag{2}$$

where $f_i : Q \to \mathbb{R}, i = 1, \ldots, k$, is called the i-th objective of the MOP. The domain Q can be expressed as

$$Q := \{x \in \mathbb{R}^n \ : \ g_i(x) \leq 0, \ i = 1, \ldots, m, \ h_j(x) = 0, \\ j = 1, \ldots, p\}, \tag{3}$$

where the g_i's denote the inequality constraints and the h_j's the equality constraints.

The optimality of a MOP is defined by the concept of *dominance*.

Definition 1

(a) Let $v, w \in \mathbb{R}^k$. Then the vector v is *less than* w ($v <_p w$), if $v_i < w_i$ for all $i \in \{1, \ldots, k\}$. The relation $\leq_p$ is defined analogously.
(b) A vector $y \in Q$ is *dominated* by a vector $x \in Q$ ($x \prec y$) with respect to Eq. 1 if $F(x) \leq_p F(y)$ and $F(x) \neq F(y)$, else y is called non-dominated by x.
(c) A point $x \in Q$ is called *(Pareto) optimal* or a *Pareto point* if there is no $y \in Q$ which dominates x.
(d) The set P_Q of all Pareto optimal solutions is called the *Pareto set* and its image $F(P_Q)$ the *Pareto front*.

So far, many different methods have been proposed to approximate the Pareto set/front of a given MOP. Scalarization methods, for instance, transform the MOP into a clever sequence of scalar optimization problems (SOP), such that a finite size discretization of the solution set can be computed (e.g., [14, 19, 38]). Continuation methods perform a search along the Pareto set and are very efficient if one (or more) solution is at hand [23, 34–36, 44, 56, 57]. There are also set-oriented methods such as evolutionary strategies [6, 7, 12, 15] and subdivision techniques [18, 25, 51], which instead use sets or populations that gradually approximate the solution set in one run of the algorithm.

For the treatment of MaOPs, some evolutionary algorithms have been proposed, for instance algorithms with large population sizes [24], methods based on dimension reduction techniques [49], strategies on space partitioning [2], or hierarchical approaches [21, 39, 42, 43]. However, all of these methods suffer from the "curse of dimensionality" and are not capable of computing a suitable finite size approximation of the entire solution set for large values of k.

In the following, the basics of the Pareto Tracer and the Pareto Explorer, the numerical tools utilized in this work for the treatment of MOPs and MaOPs, are described respectively.

2.2.1 Pareto Tracer

Here, the core elements of PT for unconstrained problems are stated, and for details including constraint handling, we refer to [34].

By considering the Karish-Kuhn-Tucker (KKT) equations for MOPs, one can identify a map $\tilde{F}$ such that the zero set $\tilde{F}^{-1}(0)$ contains the KKT points of Eq. 1 plus their corresponding weight vectors. The tangent space of this zero set at a given KKT point x with associated weight α is given by the kernel of

$$\tilde{F}'(x, \alpha) = \begin{pmatrix} W_\alpha & J^T \\ 0 & e \end{pmatrix} \in \mathbb{R}^{(n+1)\times(n+k)}, \tag{4}$$

where $J := J(x) \in \mathbb{R}^{k\times n}$ denotes the Jacobian of F at x, $e = (1, \ldots, 1)^T \in \mathbb{R}^k$, and

$$W_\alpha := \sum_{i=1}^{k} \alpha_i \nabla^2 f_i(x) \in \mathbb{R}^{n\times n}. \tag{5}$$

To compute such a kernel vector, let $v \in \mathbb{R}^n$ and $\mu \in \mathbb{R}^k$ such that

$$\tilde{F}'(x, \alpha) \begin{pmatrix} v \\ \mu \end{pmatrix} = \begin{pmatrix} W_\alpha & J^T \\ 0 & e \end{pmatrix} \begin{pmatrix} v \\ \mu \end{pmatrix} = \begin{pmatrix} 0 \\ 0 \end{pmatrix}. \tag{6}$$

By the second equation in Eq. 6, it follows that

$$\sum_{i=1}^{k} \mu_i = 0, \tag{7}$$

and by the first equation – assuming that W_α is regular – that

$$v_\mu = -W_\alpha^{-1} J^T \mu. \tag{8}$$

Note that v_μ depends on μ which is still not determined. The following discussion shows that μ can be used to steer the search in objective space. First, take into account that a movement in direction v in decision space leads to a movement Jv in objective space (e.g., [46]). Then, assuming that a vector $d \in \mathbb{R}^k$ is given, a vector $v_d \in \mathbb{R}^k$ with $J v_{\mu_d} = d$ can be obtained using Eq. 8) via

$$J v_{\mu_d} = -J W_\alpha^{-1} J^T \mu_d = d. \tag{9}$$

Since further μ_d has to satisfy Eq. 7, μ_d is completely determined by solving

$$\begin{pmatrix} -J W_\alpha^{-1} J^T \\ e \end{pmatrix} \mu_d = \begin{pmatrix} d \\ 0 \end{pmatrix}. \tag{10}$$

It remains to choose proper directions d in objective space. For this, it can be used the fact that the weight α is orthogonal to the linearized Pareto front at $F(x)$ [23]. It thus makes sense to choose d orthogonal to α in order to steer along the Pareto front: let $\alpha = QR = (q_1, \ldots, q_k)R$ a QR-factorization of α, then set

$$d_i := q_{i+1}, \quad i = 1, \ldots, k-1, \tag{11}$$

and compute the μ_{d_i}'s via Eq. 10. Then the resulting vectors $v_{\mu_{d_i}}$ are tangential to the Pareto set, and the according directions in objective space are given by the d_i's.

PT is a predictor-corrector method that uses the above described tangent vectors for the prediction step. For the corrector, it utilizes the Newton method proposed in [20], where the Newton direction is computed via solving

$$\begin{aligned} \min_{(v,\delta)\in\mathbb{R}^n\times\mathbb{R}} \quad & \delta \\ \text{s.t.} \quad & \nabla f_i(x)^T v + \frac{1}{2} v^T \nabla^2 f_i(x) v \leq \delta, \quad i = 1, \ldots, k. \end{aligned} \tag{12}$$

Since W_α is used, the resulting PC method requires Hessian information of all objectives in each step. This requirement, however, can be reduced to the sole use of the Jacobians when approximating W_α via quasi-Newton updates.

2.2.2 Pareto Explorer

In case the number k of objective is too high, it is not possible to compute a suitable finite size approximation of the entire solution set any more. Instead, the Pareto Explorer [47] aims to find a solution in cooperation with the decision maker (DM) in two steps

(Step 1) Compute a solution x_0 of the MaOP.
(Step 2) Explore the Pareto landscape around x_0 via performing movements into user specified directions.

Step 1 can be performed via a global heuristic such as an evolutionary reference point method. For Step 2, the above described PT has been adapted in [47] that allows to perform best fit movement along the Pareto set/front in directions defined in decision, objective, and weight space. The key for this is the fact that the tangent spaces of both the Pareto set at x and the Pareto front at $F(x)$ can be computed for every regular solution x which follows by the above discussion (computation of the predictor for PT). By doing so, Step 2 allows for a fine-tuning of the initial solution x_0 from Step 1.

Figure 1 shows a hypothetical example for a best fit movement along the Pareto front from the image $F(x_i)$ at the current iterate x_i. Hereby, $d_y \in \mathbb{R}^k$ denotes the desired direction in objective space specified by the DM, and $d_y^{(i)} \in \mathbb{R}^k$ the direction projected to the linearized Pareto front at $F(x_i)$. The projected direction $d_y^{(i)}$ is used to perform a best fit movement along the Pareto front of the problem. Note that the resulting path of solutions x_i resembles a path (i.e., a one-dimensional object) regardless of the number k of objectives.

3 The model

In the following, the many objective PIM model consisting of seven objectives that are used for this study is described . Further on, a plastic gear that is utilized as demonstrator for the application of the Pareto Explorer is presented .

3.1 Design parameters

The process parameters considered here are the melt temperature (T_{melt}), the packing time (t_{pack}), the packing pressure (P_{pack}), and the cooling time (t_{cool}), which are briefly defined as follows:

- x_1: *Melt temperature* (T_{melt}): the temperature of the plastic melt as it enters the mold.
- x_2: *Packing time* (t_{pack}): the period of time where additional plastic is injected into the cavity to compensate for inherent shrinkage during injection phase.
- x_3: *Packing pressure* (P_{pack}): the pressure exerted on the melt entrance during the packing phase. In this case, P_{pack} is considered as the packing pressure applied over the effective packing time, t_1=0.5t_{pack}, in a packing pressure profile. Figure 2 illustrates an example of a pressure profile.
- x_4: *Cooling time* (t_{cool}): the period of time after packing phase and before the mold opening and part ejection. It can represent up to 50% of the cycle time.

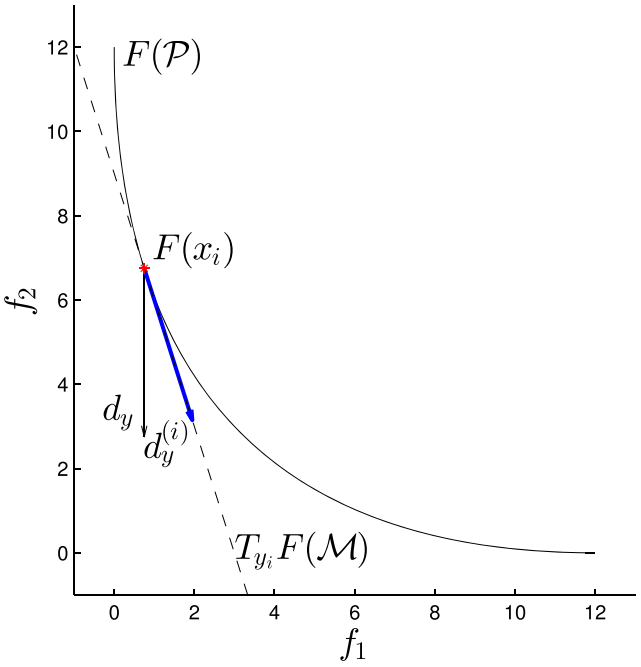

Fig. 1 Best fit direction $d_y^{(i)}$ for a given direction d_y in objective space for the Pareto Explorer

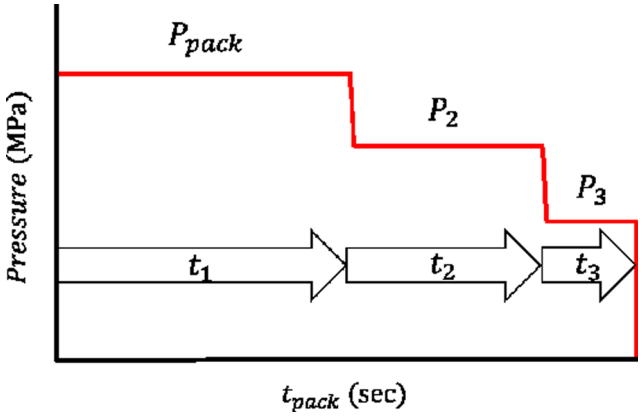

Fig. 2 Packing pressure profile

These process parameters are the most frequently used parameters considered in previous works (e.g., [26–28, 32, 33, 41, 52, 53, 55, 61, 62] and references therein).

3.2 Objectives

The outcomes of interest (or objectives) are related to the quality and productivity of the PIM process. The quality is measured by means of cosmetic and functional characteristics, while productivity is measured by indicators such as processing time and energy usage. Cosmetic characteristics are measured by means of *warpage* in the product, *shrinkage*, and *sink marks*. Commonly, these objectives are considered in other works [26, 27, 41, 52, 55, 61, 62]. Functional properties are represented by residual stresses such as *Von Mises* and *shear* stresses [3, 5, 48]. Productivity is measured by the *cycle time* and *clamping force* usage [26, 27, 33, 41, 52, 61]. Likewise, these outcomes are briefly described next:

- f_1: *Warpage* (mm): produced by non-uniform shrinkage in the plastic part. Besides, by temperature differences from one side of the mold to the other. It is mainly affected by packing time and cooling time.
- f_2: *Volumetric shrinkage* (%): all plastic parts tend to shrink; however, it is desired to have a minimum and uniform shrinkage. Non-uniform volumetric shrinkage leads to warpage and distortion of molded parts. High values may lead to sink marks or voids. It shows the percentage of part volume as the part is cooled from high temperature and high pressure to room conditions. Positive values represent volume shrinkage while negative values means volume expansion. It is affected by melt temperature, packing pressure, and cooling time.
- f_3: *Sink marks* (mm): Plastic parts could present sink marks in the finished look. Higher values of this means high degree on sink. It is an index to evaluate the packing effect. If it is positive, meaning packing is not enough, leading to sink marks. If it is negative, it means overpacking. A well packing keeps the indicator close to zero. It is affected by packing pressure and packing time.
- f_4: *Von Mises stress* (MPa): the Von Mises thermal residual stress of the ejected part. Thermal induced residual stress is the stress status after the part is ejected and cooled down to room temperature. Non-uniform volumetric shrinkage will cause residual stress if it did not transform into warpage. Higher values of residual stress cause void defects. Von Misses stress is the scalar that represents the equivalent stress used for breakage test of the product, which is defined with the stress components for each axis. It is affected by melt temperature and cooling time.
- f_5: *Shear stress* (%): the source of the residual stress in molded parts. If the shear stress is not distributed evenly, it can cause some dimensional problems. Too high shear stress might tend to drastically deform molecular chains even to break and then weaken the strength of the plastic part. It is mainly affected by melt temperature.
- f_6: *Cycle time* (seconds): the total time of a process run, this includes the filling time, mold opening time, packing time, and cooling time. It is affected by packing and cooling times which can represent up to 70% of total cycle time.
- f_7: *Clamping force* (Ton): the maximum force of machine (clamping unit) to keep the mold closed against the cavity pressure during injection/packing phases. It can be considered as great influence for energy saving. It is affected by packing pressure and packing time.

3.3 Case study: a plastic gear

As a case study in this work, it utilized the design of a particular plastic gear. Figure 3 shows the chosen plastic gear with dimensions 25.01 × 24.87 × 5.00 mm. An overview of the molding die, runner system, and cooling channels is shown in Fig. 4.

A finite element (FE) model containing 32,025 elements is developed for simulating the injection molding process in MOLDEX3D R15 2018 (www.moldex3d.com). The material used is a type of polypropylene (PP) supplied by A. Schulman whose trade name is POLYFLAM RPP 374ND CS1. The properties of the material are listed in Table 1. The process parameters, their ranges, and units, utilized as design variables, are listed in Table 2. Tables 3, 4, and 5 list the rest of the process parameters considered during the numerical simulation. Similarly, Table 6 lists the outcomes

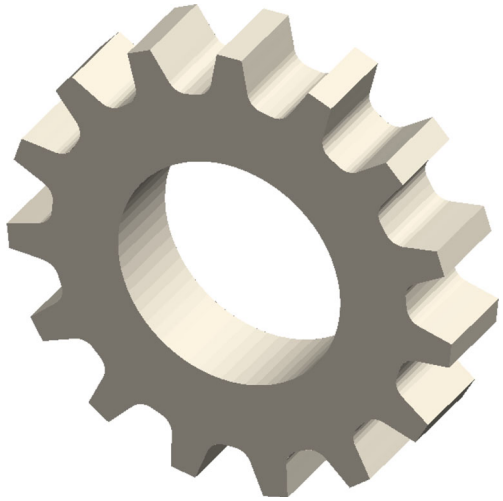

Fig. 3 Plastic gear

of interest. Figure 5 illustrates an example of the warpage scale in the simulation software.

3.3.1 Building the model

The main goal of a surrogate model is to be as accurate as possible via using as few samples as possible. One of the major steps on the process of constructing a surrogate model is the sample collection. In this work, there are a total of 150 samples collected at selected values of $x \in D$, where

$$D := \left\{ x \in \mathbb{R}^4 : \begin{array}{c} 190 \le x_1 \le 230 \\ 3 \le x_2 \le 5 \\ 60 \le x_3 \le 100 \\ 8 \le x_4 \le 14 \end{array} \right\}. \tag{13}$$

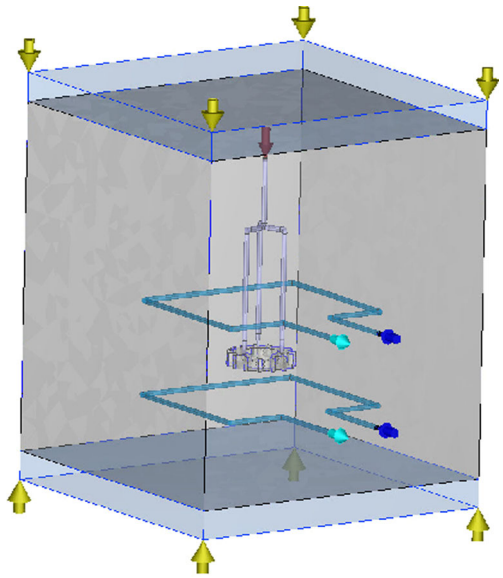

Fig. 4 Overview of molding die, runner system, and cooling channels

Table 1 Material properties of PP

Density [g/cm^3]	1.35
Eject temperature [°C]	90
Thermal conductivity [erg/(sec cm °C)]	35000
Elastic modulus [dyne/cm^2]	3e+010
Poisson ratio	0.38
Heat capacity [erg/(g °C)]	1.5e+007
Melt temperature range [°C]	200–220
Mold temperature range [°C]	40–80

Table 2 Design variables

Process parameter	Design variable	Range
Melt temperature [°C]	x_1	190–230
Packing time [sec]	x_2	3–5
Packing pressure [MPa]	x_3	84–140
Cooling time [sec]	x_4	8–14

Table 3 Process parameters

Process parameter	Value
Filling time [sec]	0.10
Mold temperature [°C]	60.0
Maximum pressure machine [MPa]	140.00
Injection volume [cc]	1.89
VP switch by volume filled [%]	98.00
Mold opening time [sec]	5.00
Ejection temperature [°C]	90.0
Air temperature [°C]	25.0

Table 4 Flow rate profile

Section	Time [%]	Flow rate [%]
1	20	30
2	40	60
3	80	90
4	100	30

Table 5 Packing rate profile

Section	Time [%]	Flow rate [MPa]
1	50	x_3
2	80	70
3	100	35

Table 6 Objective functions

Outcome	Function	Optimization
Maximum warpage deformation [mm]	f_1	Minimize
Maximum volumetric shrinkage [%]	f_2	Minimize
Maximum Von Mises stress [MPa]	f_3	Minimize
Sink marks displacement [mm]	f_4	Minimize
Maximum claming force [ton]	f_5	Minimize
Cycle time [sec]	f_6	Minimize
High shear stress [%]	f_7	Minimize

Table 7 Objective functions

Function	Surrogate model	R^2 training	R^2 testing
f_1	Quadratic	0.99	0.99
f_2	Quadratic	0.99	0.99
f_3	Shallow neural network	0.98	0.93
f_4	Quadratic	0.98	0.98
f_5	Shallow neural network	0.82	0.89
f_6	Linear	1.00	1.00
f_7	Quadratic	0.93	0.93

to evaluate $y \in \mathbb{R}^7$ via D-optimal [8, 50] and Latin hypercube [37] experimental designs. Hence, these samples are used to generate surrogate models of $f_i, i = 1, \ldots, 7$, of the outcomes of interest which make them suitable for an optimization algorithm.

Generation of a surrogate model can be seen as a multi-dimensional non-linear optimization problem which can be solved via least squares. Therefore, the problem can be formally defined as

$$\min_{\beta} \| f(x, \beta) - y \|_2^2 = \min_{\beta} \sum_i (f(x_i, \beta) - y_i)^2, \tag{14}$$

where x is the input sample vector, y is the output sample vector, β is the parameter vector, and f is the surrogate model. The problem presented in Eq. 14 can be solved using different methods [30, 59]. Polynomial and artificial neural networks models [1, 4, 11, 13, 29, 31, 40, 54, 58, 60] represent some of the most popular surrogate models in engineering. Table 7 shows the results of the surrogate models generated for each one of the outcomes of interest.

4 Numerical results

In this section, there are some numerical results presented for hypothetical scenarios of the PIM design. For this, it is first considered selected sub-problems with two and three objectives. The consideration of these MOPs might be interesting in case the decision maker has a strong preference on just a few objectives. Further, the results show that all the objectives are indeed in conflict and that the entire problem consisting of seven objectives cannot be treated any more with traditional methods. In the second sub-section, some numerical results of the Pareto Explorer on the seven-objective MaOP on selected scenarios are shown.

4.1 Multi-objective PIM design

When considering a MOP (i.e., a problem with two or three objectives), one is interested in a suitable finite size approximation of the entire Pareto front as this offers the decision maker a good overview of the possible optimal

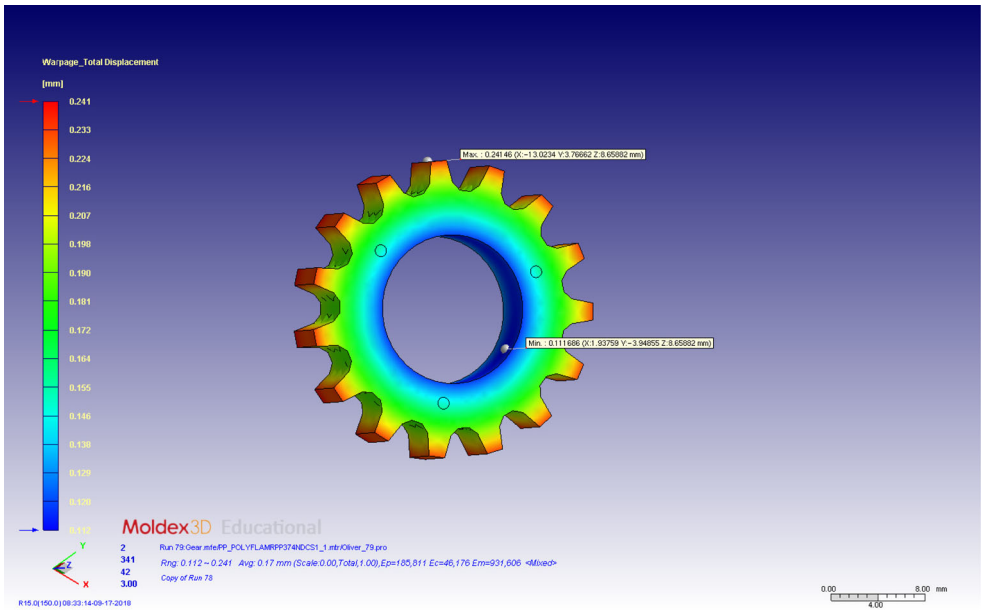

Fig. 5 Warpage in the plastic part

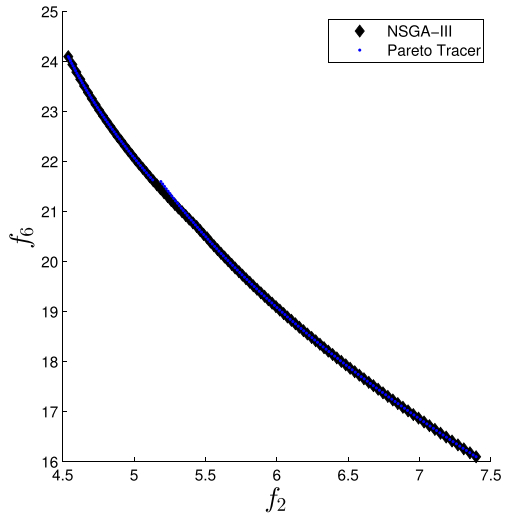

Fig. 6 Obtained Pareto fronts by PT and NSGA-III for the MOP defined by f_2 and f_6

Table 8 Parameters of the selected MOEAs

Algorithm	Parameter	Value
NSGA-III	Population size	92
	Reference points	91
	Crossover probability	1
	Mutation probability	$1/n$
	Distribution index for crossover	20
	Distribution index for mutation	20
PT	τ	0.01
	x_0	$(210.00, 4.00, 80.00, 11.00)^T$

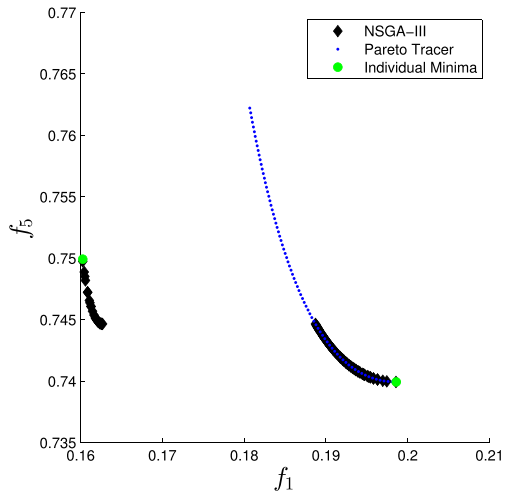

Fig. 7 Obtained Pareto fronts by PT and NSGA-III for the MOP defined by f_1 and f_5

designs. The choice of the solver depends in this case on the surrogate model. If all objectives are linear or quadratic, one can expect that the Pareto front consists of one connected component, and a local solver such as PT can be chosen. If at least one objective is expected to be multi-modal, then the Pareto front may fall into several connected components, and a global solver such as an evolutionary algorithm may be of advantage. This is demonstrated on two examples.

First, the MOP that is defined by the two objectives f_2 (quadratic) and f_6 (linear) is considered. Figure 6 shows the numerical results of the PT and the evolutionary algorithm NSGA-III [16]. See Table 8 for the chosen parameter setting of both algorithms. NSGA-III and PT yield almost identical results and are capable of approximating the Pareto front perfectly. A huge difference, however, is in the computational effort needed to compute the results. NSGA-III is given a budget of 50,000 function evaluations. In contrast, PT required 190 function and another 190 Jacobian calls. If counting one Jacobian call by 4 function evaluations (as this can be done if the Jacobians were evaluated via automatic differentiation [22]), then the PT result would have been obtained via total of less than 1,000 function evaluations which is significantly less as for the evolutionary algorithm.

Second, the MOP that is defined by f_1 (quadratic) and f_5 (defined by neural network model and multi-modal). Figure 7 shows the results obtained by PT and NSGA-III. Again, PT spends much less function evaluations (around 4,000 counting one Jacobian call as 4 function calls as above) than NSGA-III (50,000). However, as PT was run with one single starting point, it only detects one part of the Pareto front that consists of 2 connected components. As it does not detect the 2nd component, it computes also some solutions that are only locally optimal. NSGA-III, on the other hand, is capable of detecting both components and delivers a suitable approximation of the solution set.

Some other Pareto fronts for other sub-problems can be seen in Fig. 8.

Finally, a three-objective problem defined by the objectives f_1, f_5, and f_6 is considered . Since f_5 is multi-modal, it is first run NSGA-III to obtain a rough approximation of the two-dimensional Pareto front, see Fig. 9. In order to refine the obtained solutions, PT is applied where it was fed this algorithm with each of the individuals from the final population of NSGA-III. As it can be seen, a much better approximation of the entire Pareto front can be obtained. To obtain this result, it has been given NSGA-III a budget of 150,000 function calls which has led to 100 non-dominated solutions. In the second step, PT has used 64,369 function evaluations and 5877 Jacobian evaluations (leading to 87877 function evaluations when using automatic differentiation) leading to a total of 1948 non-dominated solutions. It is thought that this combination is most effective for three-objective problems that is confirmed with other computations.

From all results, it can be seen that all objectives are in conflict with each other. Thus, one cannot expect to be able to compute suitable finite size approximations of the entire Pareto set/front for problems with more objectives. That is the reason the applications of the Pareto Explorer are considered for this case in the next section.

4.2 Many objective PIM design

Here, the entire design problem that consists of seven objectives is examined. As one cannot expect any more to compute suitable approximations of the entire solution set (which can then be presented to the decision maker), it has to be restricted to some selected hypothetical scenarios that can occur. It is stressed, however, that these are just illustrators for a possible decision making. The decision-making process for a given problem will heavily depend

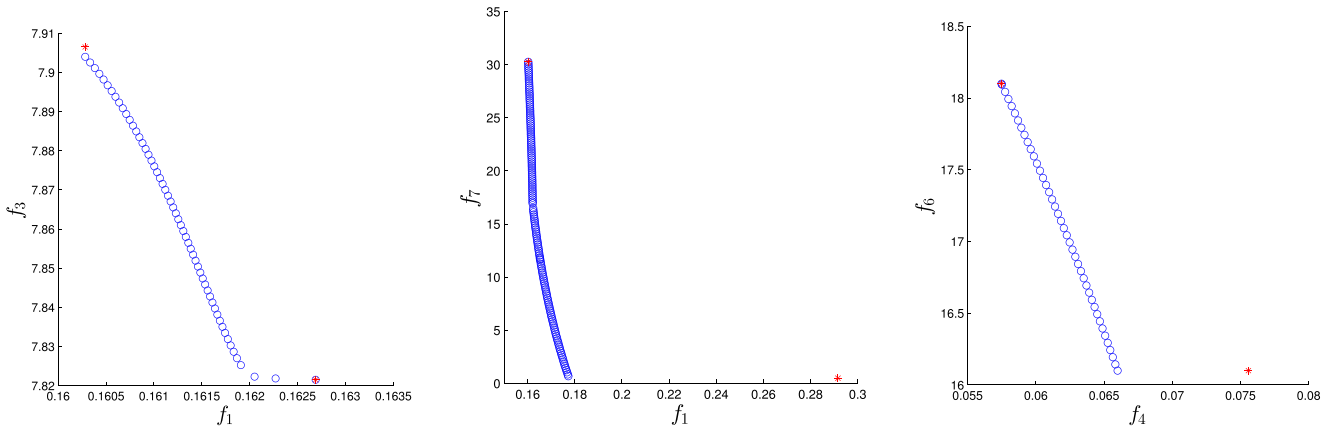

(a) f_1 and f_3 (b) f_1 and f_7 (c) f_4 and f_6

Fig. 8 Some Pareto fronts for three selected bi-objective sup-problems

Fig. 9 Example of PT and NSGA-III for f_1, f_5, and f_6

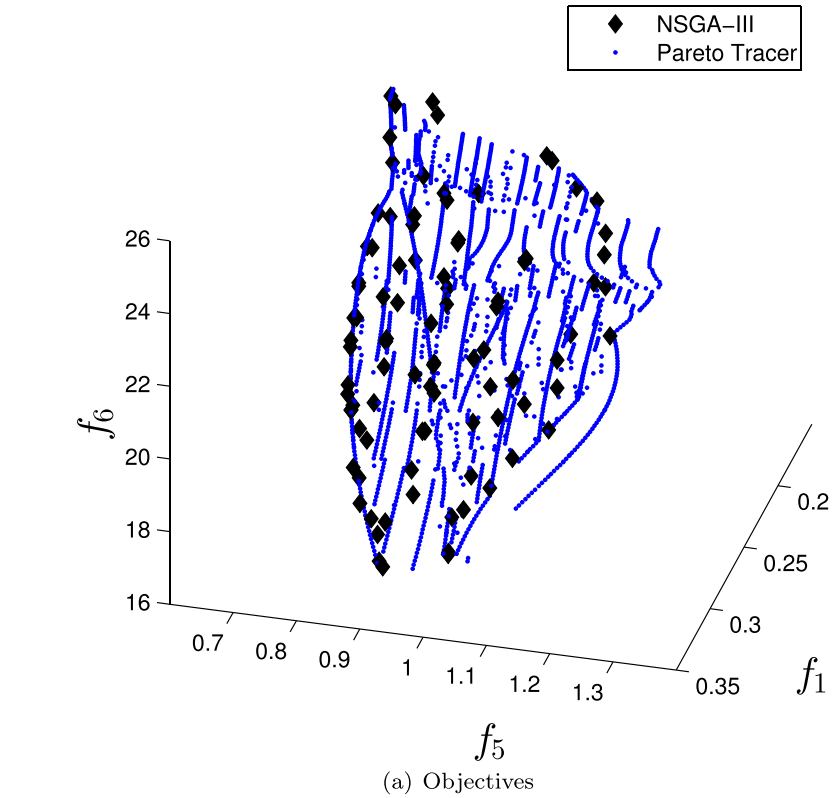

(a) Objectives

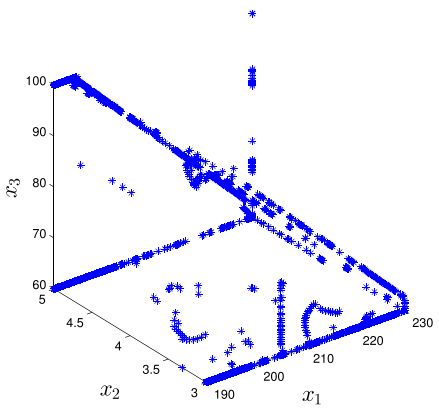

(b) x_1, x_2, x_3

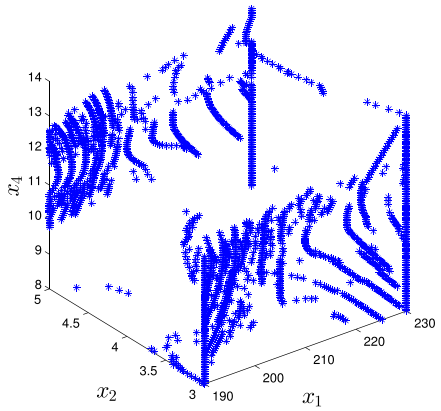

(c) x_1, x_2, x_4

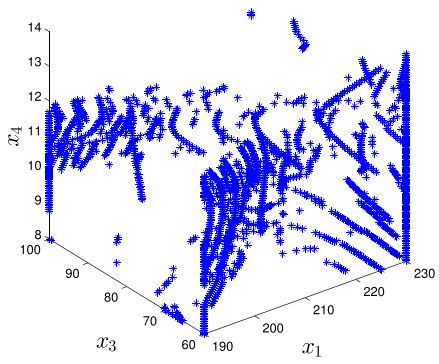

(d) x_1, x_3, x_4

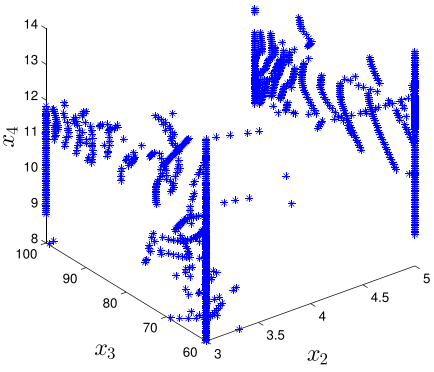

(e) x_2, x_3, x_4

Table 9 Computational cost of the PE for the Scenarios 1–4

	S1	S2	S3	S4
Solutions	323	218	212	205
Function evaluations	324	226	227	217
Jacobian evaluations	324	226	227	217

Table 10 Comparison of the model values (F_M) against the simulated values F_S for the PIM

Initial configuration							
x_0	210.0000	4.0000	80.0000	11.0000			
$F_S(x_0)$	**0.2016**	5.6565	9.7470	0.0717	**0.8690**	20.1000	11.9460
$F_M(x_0)$	**0.2040**	5.7271	9.7329	0.0713	**0.8774**	20.1000	11.8221
Case 1							
x_{323}	230.0000	3.0000	60.0000	13.0163			
$F_S(x_{323})$	**0.1887**	5.2977	8.3664	0.0854	**0.7680**	21.1163	12.4440
$F_M(x_{323})$	**0.1896**	5.3191	8.1392	0.0854	**0.7437**	21.1163	12.9238
Case 2							
x_{218}	212.7412	3.3488	60.0000	9.6531			
$F_S(x_{218})$	0.2442	**6.5442**	9.2361	0.0769	1.0300	**18.1019**	7.4741
$F_M(x_{218})$	0.2425	6.4453	9.6549	0.0767	0.9258	**18.1018**	11.7376
Case 3							
x_{212}	213.3452	3.3421	60.0000	9.6950			
$F_S(x_{212})$	**0.2437**	6.5210	9.1729	0.0772	**1.0300**	**18.1371**	7.9492
$F_M(x_{212})$	**0.2419**	6.4289	9.6057	0.0770	**0.9199**	**18.1371**	11.7847
Case 4							
x_{205}	217.3894	3.2880	60.7034	9.8649			
$F_S(x_{205})$	0.2414	6.4710	**9.1775**	0.0787	**1.0100**	**18.2529**	8.9651
$F(x_{205})$	0.2404	6.3740	9.4653	0.0787	**0.8806**	18.2529	11.7933

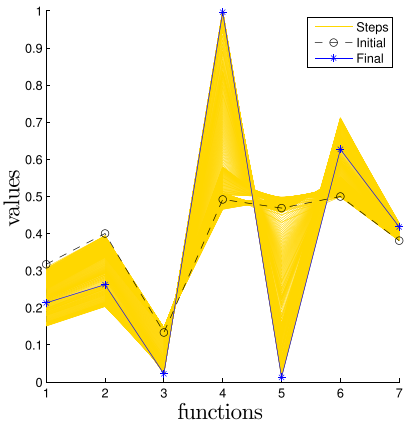

(a) Line plot

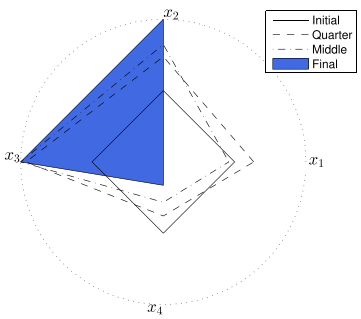

(b) Pareto Set

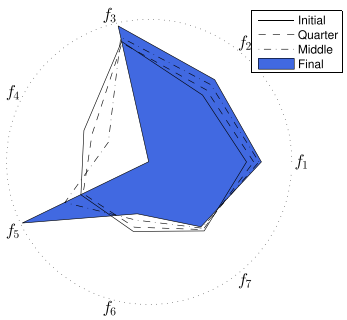

(c) Pareto Front

Fig. 10 Graphical result for the first scenario

on the given setting and on the preferences of the decision maker.

For all cases, it has been chosen to take $x_0 = (210.00, 4.00, 80.00, 11.00)^T$ as initial solution, which is the middle point for each variable in the considered range of the sampling process. Hence, x_0 is chosen as initial solution for Step 1 of the PE. This is done for simplicity and to have the same starting point for all scenarios and to show the effect of the different steerings. It is stressed, however, that in principle any other starting point could be taken or computed. For the demonstration of Step 2 of the PE, there are considered the following four scenarios:

Scenario 1 (S1): For this scenario, it is intended to minimize the values of f_1 and f_5 at the same time. Thus, the direction that is considered is $d_y = (-1, 0, 0, 0, -1, 0, 0)^T$ with a step size $\tau = 0.03$. That is, it is of interest solutions that reduce both the warpage and the shear stress (in the same amount) during the search along the Pareto front.

Scenario 2 (S2): Here, the goal is to minimize f_2 and f_6 at the same time. Thus, the direction that is considered is $d_y = (0, -1, 0, 0, 0, -1, 0)^T$ with a step size $\tau = 0.01$.

Scenario 3 (S3): Here, it is wanted to minimize the functions f_1, f_5, and f_6 at the same time. The considered direction is then $d_y = (-1, 0, 0, 0, -1, -1, 0)^T$ with a step size $\tau = 0.01$.

Scenario 4 (S4): Finally, it is desired to minimize the functions f_3, f_5, and f_6 at the same time. The direction is thus $d_y = (0, 0, -1, 0, -1, -1, 0)^T$ with a step size $\tau = 0.01$.

The computational cost of these scenarios are presented in Table 9 and a comparison of the values with our model and the values with the simulator are presented in Table 10.

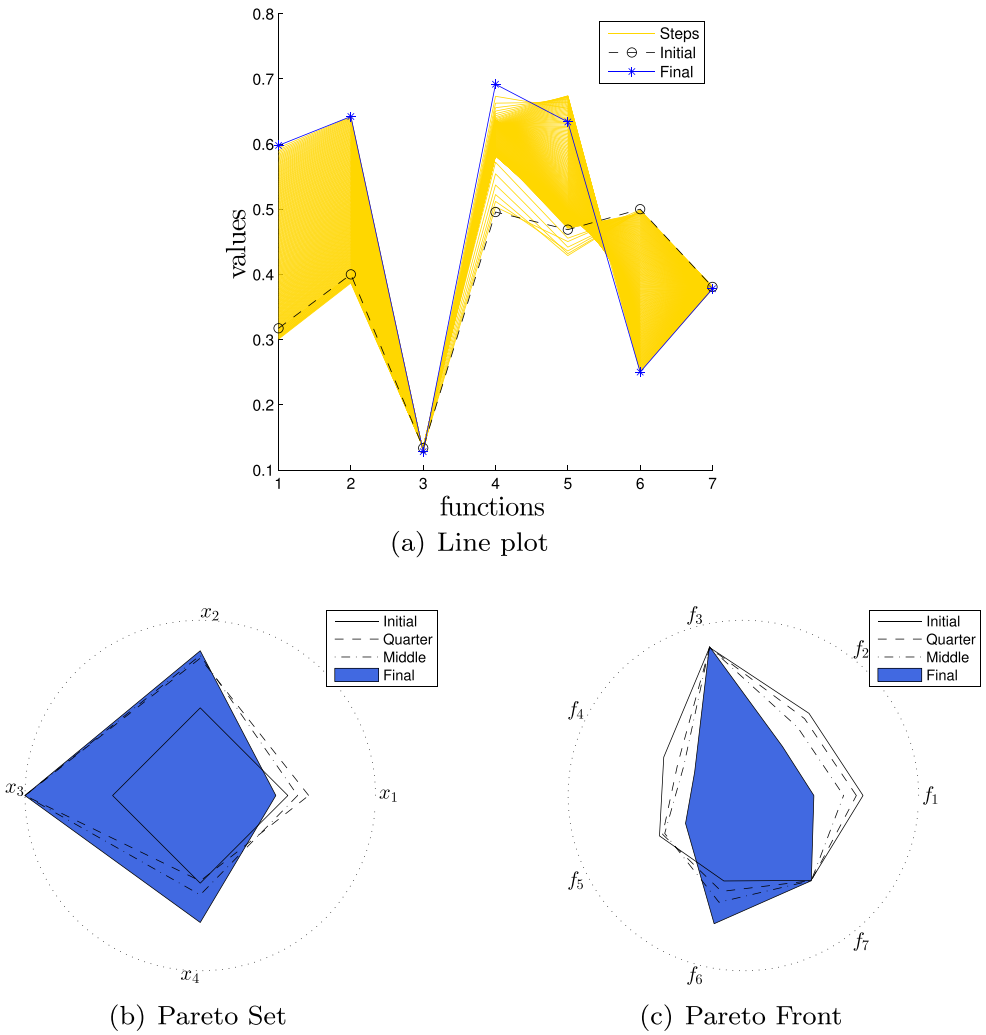

(a) Line plot

(b) Pareto Set

(c) Pareto Front

Fig. 11 Graphical result for the second scenario

It can be seen from Fig. 10 that both f_1 and f_5 improve their values with respect to the initial $F(x_0)$. However, at the end of the optimization process, obtained the best value for f_5 is considered , while for f_1 the best value was reached in a previous step.

It is seen in Fig. 11 that the functions f_2 and f_6 are clearly in conflict. Then, when it is reduced, the value of f_6, the value of f_2 begins to increase. At the end of the optimization process, the best value for f_6 and the worst value for f_2 are obtained.

It is seen in Fig. 12 that the functions f_1 and f_6 are directly in conflict, while f_5 the value depends of both functions. At the end of the optimization process, the best value for f_6 and the worst value for f_1 are obtained; for the case of f_5 the initial and the final values are similar, but along the steps such value has a lot of variation. Notice that the result for this scenario is almost the same than the previous one.

It can be seen in Fig. 13 that PE reduces two of the three functions. It is noticed that the values of f_6 and f_3 are always reduced, while the change in f_5 is not constant. At the end of the optimization process, the best value for f_3 and f_6 is obtained, while the best values for f_5 is obtained in a previous step. However, notice that in some step the value of f_1, f_5, and f_6 are improved with respect of the initial one.

As it can be seen, the movement has been performed in all cases according to the desired direction. It has been presented here the entire path of solutions; however, in a real decision-making process, the DM can of course chose at any time either to accept a computed candidate solution or to change the direction in which the steering has to be performed.

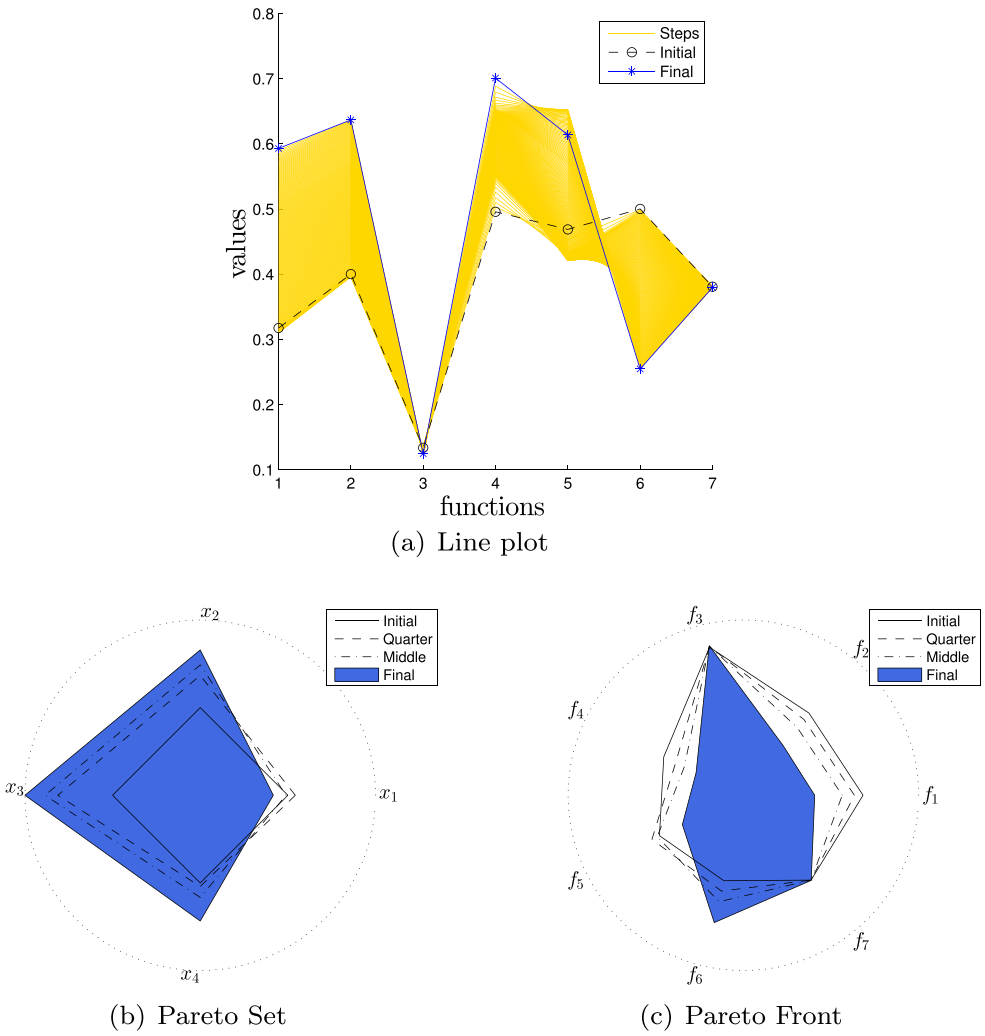

(a) Line plot

(b) Pareto Set

(c) Pareto Front

Fig. 12 Graphical result for the third scenario

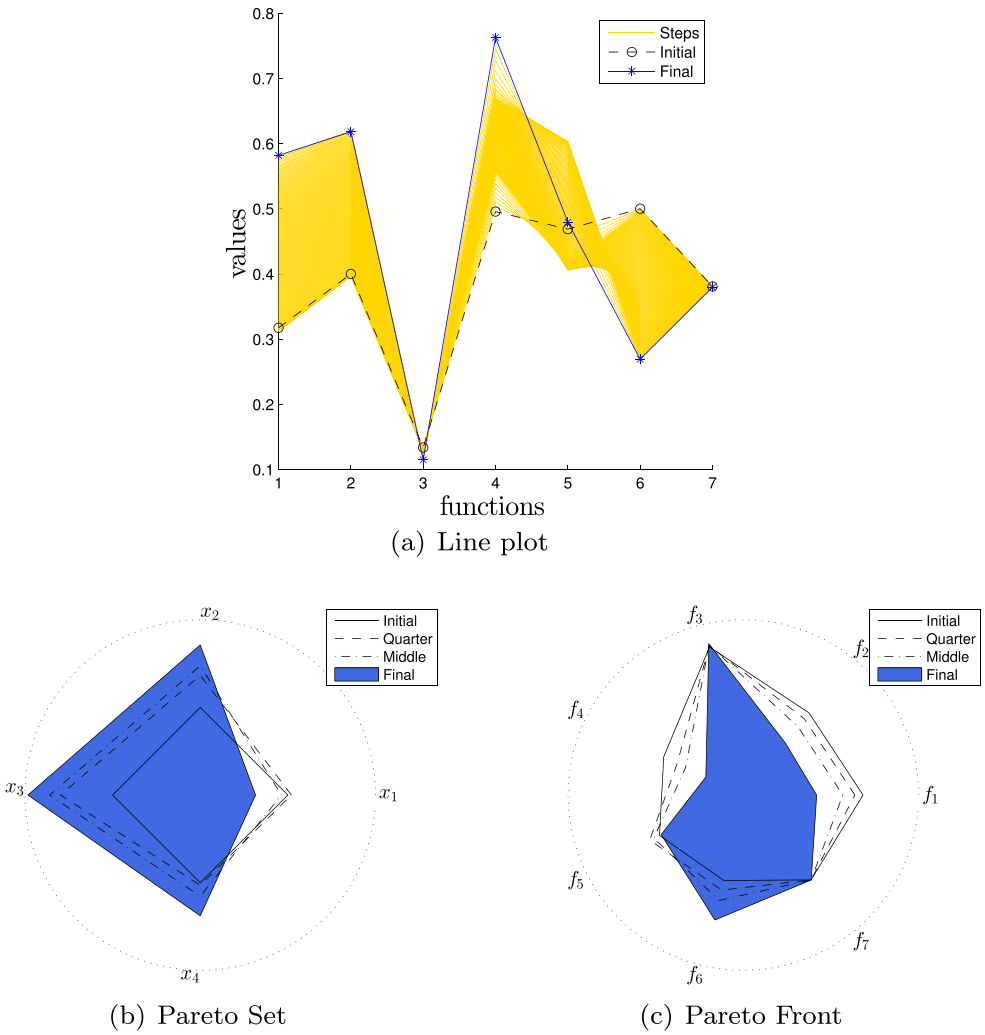

Fig. 13 Graphical result for the last scenario

(a) Line plot

(b) Pareto Set

(c) Pareto Front

5 Conclusions and future work

In this paper, it has been for the first time that the many objective design of a plastic injection molding process are considered. For this, a model that consists of seven objectives that all have a potential significant impact on the decision-making process and that are in conflict to each other has been proposed . The peculiarity of multi-objective and many objective optimization problems is that their solution sets, the Pareto sets, and Pareto fronts typically form $(k-1)$-dimensional objects, where k is the number of objectives considered in the problem. Hence, it is

not possible any more for $k = 7$ to compute suitable finite size approximations of the entire Pareto sets/fronts.

It has been demonstrated on the case study of a particular plastic gear that the Pareto fronts of related MOPs can be reliably computed either via a continuation-like method or a global search heuristic depending on the type of the surrogate model. More precisely, the Pareto Tracer can be chosen for linear and/or quadratic models, while the evolutionary algorithm NSGA-III is preferred over the local method for multi-modal models that typically arise from neural network models. For problems with $k = 3$ objectives, a combination of both techniques led to the best results.

When considering the complete model ($k = 7$), none of these classical methods can be chosen any more due to the "curse of dimensionality" as described above. As alternative, it has been proposed to utilize the Pareto Explorer, a global/local method that iteratively finds new candidate solutions along the Pareto set/front depending on the decision makers preferences. For this, four different scenarios were investigated , and in all cases a movement from the initial solution into the desired search direction has been observed.

It is conjectured from these results that the Pareto Explorer can serve as a powerful tool for the many objective design of plastic injection molding.

Future work on the plastic injection molding process must focus on the integration of design variables related to product design, mold design, material selection, and process

parameters setting. Besides, it is desired to consider as many objectives as a case study to make it possible (acceptable simulation time). Further, the PE implementation can be extended to illustrative cases to handle movements in directions in decision space and weight space in order to increase the set of alternatives given the preferences of the decision maker.

Funding The authors acknowledge support from Conacyt Basic Science project no. 285599.

References

1. Aghazadeh F, Tahan A, Thomas M (2018) Tool condition monitoring using spectral subtraction and convolutional neural networks in milling process. Int J Adv Manuf Technol 98:3217–3227
2. Aguirre H, Tanaka K (2009) Many-objective optimization by space partitioning and adaptive ε-ranking on mnk-landscapes. In: Evolutionary multi-criterion optimization. Springer, pp 407–422
3. Alvarado-Iniesta A, Guillen-Anaya LG, Rodriguez-Picon LA, Neco-Caberta R (2018) Multi-objective optimization of an engine mount design by means of memetic genetic programming and a local exploration approach. J Intell Manuf. https://doi.org/10.1007/s10845-018-1432-9
4. Ayeb M, Frija M, Fathallah R (2018) Prediction of residual stress profile and optimization of surface conditions induced by laser shock peening process using artificial neural networks. Int J Adv Manuf Technol. https://doi.org/10.1007/s00170-018-2883-z
5. Bahktiari H, Karimi M, Rezazadeh S (2016) Modeling, analysis and multi-objective optimization of twist extrusion process using predictive models and meta-heuristic approaches, based on finite element results. J Intell Manuf 27:463–473
6. Beume N, Naujoks B, Emmerich M (2007) Sms-emoa: multiobjective selection based on dominated hypervolume. Eur J Oper Res 181:1653–1669
7. Bogoya JM, Vargas A, Cuate O, Schütze O (2018) A (p,q)-averaged Hausdorff distance for arbitrary measurable sets. Math Comput Appl 23:1–24
8. Box MJ, Draper NR (1971) Factorial designs, the $|X^T X|$ criterion, and some related metrics. Technometrics 13:731–742
9. Bryce DM (1996) Plastic injection molding: manufacturing process fundamentals, vol 1. Society of Manufacturing Engineers, Dearborn
10. Carender J (2011) Injection molding troubleshooting guide, 3rd edn. Createspace Independent Publishing, Scotts Valley
11. Chen Y, Jin Y, Jiri G (2018) Predicting tool wear with multi-sensor data using deep belief networks. Int J Adv Manuf Technol 99:1917–1926
12. Coello C, Lamont GB, van Veldhuizen DA (2007) Evolutionary algorithms for solving multi-objective problems. Springer, Berlin
13. Dakhli M, Boulila A, Manach PY, Tourki Z (2019) Optimization of processing parameters and surface roughness of metallic sheets plastically deformed by incremental forming process. Int J Adv Manuf Technol. https://doi.org/10.1007/s00170-018-03265-x
14. Das I, Dennis J (1998) Normal-boundary intersection: a new method for generating the Pareto surface in nonlinear multicriteria optimization problems. SIAM J Optim 8:631–657
15. Deb K (2001) Multi-objective optimization using evolutionary algorithms. Wiley, New York
16. Deb K, Jain H (2014) An evolutionary many-objective optimization algorithm using reference-point-based nondominated sorting approach, part I: solving problems with box constraints. IEEE T Evolut Comput 18:577–601
17. Deb K, Sundar J (2006) Reference point based multi-objective optimization using evolutionary algorithms. In: Proceedings of the 8th annual conference on genetic and evolutionary computation, pp 635–642
18. Dellnitz M, Schütze O, Hestermeyer T (2005) Covering Pareto sets by multilevel subdivision techniques. J Optimiz Theory Appl 124:113–136
19. Eichfelder G (2008) Adaptive scalarization methods in multiobjective optimization. Springer, Berlin
20. Fliege J, Drummond LMG, Svaiter BF (2009) Newton's method for multiobjective optimization. SIAM J Optim 20:602–626
21. Gebken B, Peitz S, Dellnitz M (2018) On the hierarchical structure of Pareto critical sets. arXiv:1803.06864
22. Griewank A (1989) On automatic differentiation. In: Mathematical programming: recent developments and applications. Kluwer Academic Publishers, pp 83–108
23. Hillermeier C (2001) Nonlinear multiobjective optimization—a generalized homotopy approach. Basel, Birkhäuser
24. Ishibuchi H, Sakane Y, Tsukamoto N, Nojima Y (2009) Evolutionary many-objective optimization by NSGA-II and MOEA/D with large populations. In: IEEE international conference on systems, man and cybernetics, pp 1758–1763
25. Jahn J (2006) Multiobjective search algorithm with subdivision technique. Comput Optim Appl 35:161–175
26. Kitayama S, Natsume S (2014) Multi-objective optimization of volume shrinkage and clamping force for plastic injection molding via sequential approximate optimization. Simul Model Pract Theory 48:35–44
27. Kitayama S, Miyakawa H, Takano M, Aiba S (2017) Multi-objective optimization of injection molding process parameters for short cycle time and warpage reduction using conformal cooling channel. Int J Adv Manuf Technol 88:1735–1744
28. Kuo C, Dewantoro G, Huang C (2015) Optimization of injection-molded light guide plate with microstructures by using reciprocal comparisons. J Intell Manuf 26:677–690
29. Laouissi A, Yallese MA, Belbah A, Belhadi S, Haddad A (2018) Investigation, modeling, and optimization of cutting parameters in turning of gray cast iron using coated and uncoated silicon nitride ceramic tools. Based on ANN, RSM, and GA optimization. Int J Adv Manuf Technol. https://doi.org/10.1007/s00170-018-2931-8
30. Lawson CL, Hanson RJ (1995) Solving least squares problems. Society for Industrial and Applied Mathematics, Philadelphia
31. Li J, Laghari RA (2018) A review on machining and optimization of particle-reinforced metal matrix composites. Int J Adv Manuf Technol. https://doi.org/10.1007/s00170-018-2837-5
32. Liu J, Chen X, Lin Z, Diao S (2017) Multiobjective optimization of injection molding process parameters for the precision manufacturing of plastic optical lens. Math Probl Eng. https://doi.org/10.1155/2017/2834013
33. Lu N, Gong G, Yang Y, Lu J (2012) Multi-objective process parameter optimization for energy saving in injection molding process. J Zhejiang Univ-SC A 13:382–394
34. Martin A, Schütze O (2018) Pareto tracer: a predictor–corrector method for multi-objective optimization problems. Eng Optim 50:516–536
35. Martin B, Goldsztejn A, Granvilliers L, Jermann C (2013) Certified parallelotope continuation for one-manifolds. SIAM J Numer Anal 51:3373–3401
36. Martin B, Goldsztejn A, Granvilliers L, Jermann C (2016) On continuation methods for non-linear bi-objective optimization:

towards a certified interval-based approach. J Global Optim 64:3–16
37. McKay MD, Beckman RJ, Conover WJ (1979) A comparison of three methods for selecting values of input variables in the analysis of output from a computer code. Technometrics 21:239–245
38. Miettinen K (1999) Nonlinear multiobjective optimization. Kluwer Academic Publishers, Boston
39. Mueller-Gritschneder D, Graeb H, Schlichtmann U (2009) A successive approach to compute the bounded pareto front of practical multiobjective optimization problems. SIAM J Optim 20:915–934
40. Park JW, Kang BS (2018) Comparison between regression and artificial neural network for prediction model of flexibly reconfigurable roll forming process. Int J Adv Manuf Technol. https://doi.org/10.1007/s00170-018-3155-7
41. Park HS, Nguyen TT (2014) Optimization of injection molding process for car fender in consideration of energy efficiency and product quality. J Comput Des Eng 1:256–265
42. Peitz S (2017) Exploiting structure in multiobjective optimization and optimal control. Dissertation, Paderborn University (Germany)
43. Peitz S, Dellnitz M (2018) A survey of recent trends in multiobjective optimal control–surrogate models, Feedback control and Objective reduction. Math Comput Appl 23:1–33
44. Pereyra V, Saunders M, Castillo J (2013) Equispaced Pareto front construction for constrained bi-objective optimization. Math Comput Model 57:2122–2131
45. Rosato DV, Rosato DV, Rosato MG (2000) Injection Molding Handbook, 3rd edn. Springer, Norwell
46. Schütze O, Martín A, Lara A, Alvarado S, Salinas E, Coello C (2016) The directed search method for multiobjective memetic algorithms. Comput Optim Appl 63:305–332
47. Schütze O, Cuate O, Martín A, Peitz S (2019) Pareto Explorer: a global/local exploration tool for many objective optimization problems. Eng Optim (to appear)
48. Shi F, Lou L, Lu JG, Zhang YQ (2003) Optimisation of plastic injection moulding process with soft computing. Int J Adv Manuf Technol 21:656–661
49. Singh HK, Issacs A, Ray T (2011) A Pareto corner search evolutionary algorithm and dimensionality reduction in many-objective optimization problems. IEEE T Evolut Comput 15:539–556
50. Smith K (1918) On the standard deviations of adjusted and interpolated values of an observed polynomial function and its constants and the guidance they give towards a proper choice of the distribution of observations. Biometrica 12:1–85
51. Sun JQ, Xiong FR, Schütze O, Hernández C (2019) Cell mapping methods: algorithmic approaches and applications. Springer, Berlin
52. Tian M, Gong X, Yin L, Li H, Ming W, Zhang Z, Chen J (2017) Multi-objective optimization of injection molding process parameters in two stages for multiple quality characteristics and energy efficiency using Taguchi method and NSGA-II. Int J Adv Manuf Technol 89:241–254
53. Tsai K, Luo H (2017) An inverse model for injection molding of optical lens using artificial neural network coupled with genetic algorithm. J Intell Manuf 28:473–487
54. Ventaka-Rao K, Murthy PBGSN (2018) Modeling and optimization of tool vibration and surface roughness in boring steel using RSM, ANN and SVM. J Intell Manuf 29:1533–1543
55. Villarreal-Marroquín MG, Chen PH, Mulyana R, Santner TJ, Dean AM, Castro JM (2017) Multiobjective optimization of injection molding using a calibrated predictor based on physical and simulated data. Polym Eng Sci 57:248–257
56. Wang H (2013) Zigzag search for continuous multiobjective optimization. INFORMS J Comput 25:654–665
57. Wang H (2015) Direct zigzag search for discrete multi-objective optimization. Comput Oper Res 61:100–109
58. Wu TY, Lei KW (2019) Prediction of surface roughness in milling process using vibration signal analysis and artificial neural network. Int J Adv Manuf Technol. https://doi.org/10.1007/s00170-018-3176-2
59. Yuan JY (1996) Numerical methods for generalized least squares problems. J Comput Appl Math 66:571–584
60. Zerti A, Yallese MA, Meddour I, Belhadi S, Haddad A, Mabrouki T (2018) Modeling and multi-objective optimization for minimizing surface roughness, cutting force, and power, and maximizing productivity for tempered stainless steel AISI 420 in turning operations. Int J Adv Manuf Technol. https://doi.org/10.1007/s00170-018-2984-8
61. Zhang J, Wang J, Lin J, Guo Q, Chen K, Ma L (2016) Multiobjective optimization of injection molding process parameters based on Opt LHD, EBFNN, and MOPSO. Int J Adv Manuf Technol 85:2857–2872
62. Zhao J, Cheng G, Ruan S, Li Z (2015) Multi-objective optimization design of injection molding process parameters based on the improved efficient global optimization algorithm and non-dominated sorting-based genetic algorithm. Int J Adv Manuf Technol 78:1813–1826